AI-Driven Iterative Model for Accelerated ATC Computation under Transmission Congestion using Hybrid Forecasting, Deep Feature Compression, and Physics-Informed Optimizations

SANDEEP A. KALE[1], NITIN D. GHAWGHAWE[2]
[1]Electrical Engineering Department, JIT,
RTMNU, Nagpur, Maharashtra,
INDIA

[2]Electrical Engineering Department,
Government College of Engineering,
RTMNU, Nagpur, Maharashtra,
INDIA

Abstract: - The Modern power systems face rising complexity from demand expansion and renewable integration, requiring faster and more accurate Available Transfer Capability (ATC) estimation. Real-time congestion management is limited by traditional approaches' lack of scalability and inability to capture dynamic spatiotemporal changes. This paper suggests an integrated architecture that combines Graph Neural Networks (GNN) to describe spatial grid dependencies, Conditional Variational Autoencoders (CVAE) to reduce dimensionality, and hybrid VARMAx-LSTM to anticipate multivariate temporal trends. While Physics-Informed Neural Networks (PINNs) effectively solve optimal power flow under physical restrictions, Reinforcement learning via Proximal Policy Optimization (PPO) allows real-time control. A scalable, high-fidelity solution for real-time grid operations is demonstrated via validation on IEEE 30, 39, 57, and 118-bus systems, which demonstrates a 40% reduction in computing time, ~95% congestion prediction accuracy, and 10–15% ATC improvement.

Key-Words: - Transmission Network Congestion, Available Transfer Capability, Power System Reliability, Transmission Losses, Operational Costs, Congestion Pricing Generation Rescheduling, Artificial Intelligence.

Received: May 26, 2025. Revised: January 11, 2026. Accepted: May 11, 2026. Published: July 20, 2026.

1 Introduction

The ATC, as a decisive metric within the domain variables for the safe and economical operationalization of grids, adds even further criticalities in determining avenues or possibilities for market transactions as initiators of reliable scheduling while supporting congestion management efforts. Available Transfer Capability (ATC) is a critical metric for ensuring the safe, reliable, and economical operation of power grids, particularly in enabling market transactions and supporting congestion management. With rising renewable integration and shifting load patterns from urbanization, modern networks face increasingly complex congestion challenges, [1], [2]. Accurate yet computationally efficient ATC estimation is therefore essential. Conventional linear or simplified models struggle with nonlinear dynamics, variability, and real-time adaptability, while heuristic and optimization-based methods are often computationally expensive. These limitations reduce predictive capability, hinder proactive congestion mitigation, and ultimately constrain grid resilience and market efficiency through conservative operating margins.

This newly developed multi-stage framework integrates data-driven forecasting, deep feature compression, spatial dependency modeling, and physics-constrained optimization to overcome bottlenecks in ATC estimation. It begins with a hybrid VARMAx-LSTM model that forecasts congestion and ATC values using inputs such as historical load, weather, and grid topology. Conditional Variational Autoencoders (CVAE) compress forecasts into low-dimensional forms for efficient processing, while Graph Neural Networks (GNN) capture grid dependencies and identify congestion hotspots. Proximal Policy Optimization

(PPO) determines effective mitigation strategies, and Physics-Informed Neural Networks (PINNs) embed physical laws into OPF solutions. Together, these components enable fast, accurate, real-time ATC estimation.

2 In-Depth Review of Models used for ATC Analysis

Recent literature highlights the evolving approaches to Available Transfer Capability (ATC) assessment and optimization in renewable-dominated power systems. [1] addressed multi-area systems through coordinated congestion management, while reference [2] integrated optimal power flow in hybrid AC/DC networks, underscoring structural innovations. Reference [3] applied Monte Carlo simulations to incorporate wind uncertainty, emphasizing stochastic modeling. Reference [4] introduced dynamic modeling to capture renewable variability. In [5] initiated machine learning–based real-time ATC prediction, advancing data-driven methods. In [6] demonstrated ATC enhancement using FACTS devices for flexibility in deregulated markets.

As summarized in Table 1 (Appendix), recent research reflects the growing sophistication of ATC assessment and optimization frameworks. In reference [7] incorporated energy storage to buffer renewable intermittency, while reference [8] embedded N-1 contingency and transient stability constraints, strengthening security-oriented approaches. In reference [9] linked ATC to interregional exchanges, reference [10] demonstrated distributed FACTS for localized enhancement. Other contributions include environmental stressor modeling [11], clustering-based inspection [12], infrastructure resilience [13], and ML-based fault detection [14]. In reference [15] Energy storage helps reduce congestion and can indirectly increase ATC by balancing power flows. Innovations span bilevel optimization for wind-dominated networks [16], Achieved accurate probabilistic ATC estimation with significantly fewer scenarios, reducing computational time [17], HVDC flow control [18], defect detection. [19], and DLR-based corrective dispatch [20]. Nature-inspired and hybrid techniques—ranging from sea lion optimization [21] High fault-classification accuracy and faster model development compared to training from scratch [22], In reference [23] Reinforcement of transmission corridors improved network reliability and increased ATC. Enhanced transient stability and better system response during disturbances and faults [24], Drones improve inspection efficiency, safety, and fault detection accuracy by providing high-quality data from hard-to-reach locations [25] Improved structural resilience and reduced risk of tower collapse, contributing to more reliable power transfer [26] in reference [27] Demonstrated that line length has a significant impact on system performance and ATC-related limits. Improved dynamic response, power quality, damping of oscillations, and enhanced dynamic ATC [28] to COA-based planning [29]—further advance ATC scalability. Collectively, these works demonstrate a transition from deterministic to probabilistic, learning-driven approaches, guiding future interoperable, real-time, and resilient ATC systems.

3 Proposed Model Analysis

To address the limitations of low efficiency and high complexity in existing methods, this section introduces an Iterative Model for Accelerated ATC Computation under transmission congestion. The framework shown in Figure 1 employs a multi-stage hybrid approach combining forecasting, feature compression, and physics-informed optimization. Its first phase applies dynamic spatio-temporal forecasting by integrating Vector Autoregressive Moving Average with Exogenous Inputs (VARMAx) and Long Short-Term Memory (LSTM) networks to capture dependencies across grid parameters such as load, weather, flows, and congestion.

$$Yt = \sum A_i Yt^{-}{}_{i} + \sum Bj\varepsilon t^{-}t + DXt + \varepsilon t \tag{1}$$

where Y_t is a vector of endogenous variables (such as ATC and congestion), X_t holds exogenous variables (such as weather characteristics), A_i and B_j are matrices of coefficients, and ε_t is a white noise error process. Whereas VARMAx models efficiently describe linear interrelations, they are not quite capable of describing long-run temporal dynamics. Hence, an LSTM layer is appended to learn high-order temporal sequences. This equation is used for any IEEE bus system where one bus is a reference bus and one is slack bus. The LSTM cell updates are given via equations 2, 3, 4, 5, 6 & 7.

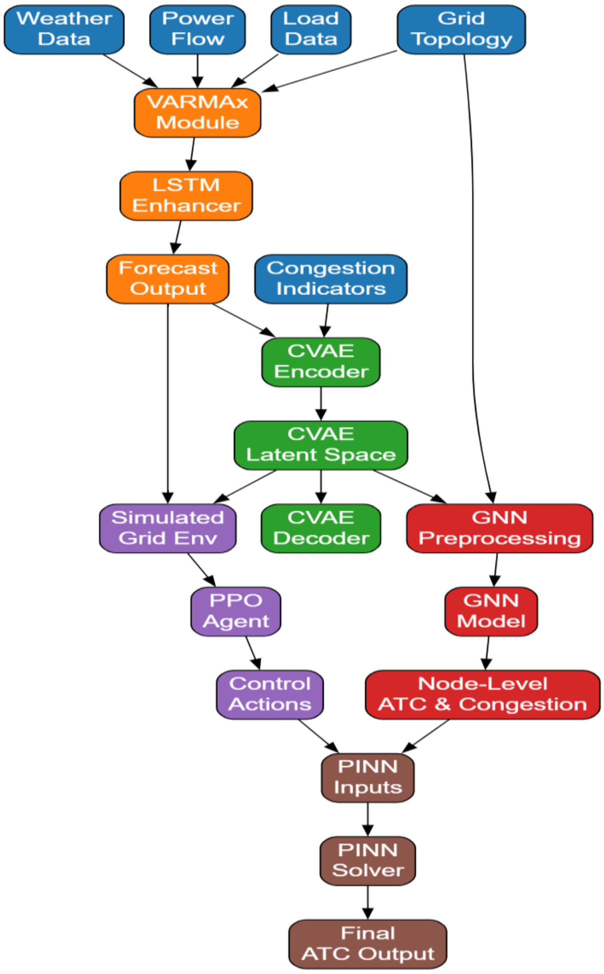

Fig. 1: Model Architecture of the Proposed Analysis Process
Source: created by the authors

Here, Y_t denotes endogenous variables (ATC, congestion), X_t represents exogenous inputs (weather), and A_i and B_j are coefficient matrices with $€_t$ as white noise. While VARMAx captures linear interrelations, LSTM layers model complex long-term temporal dependencies (Equations 2 to 7).

$$f_t = \sigma(W_f \cdot [h_{t-1}, e_t] + b_f) \quad (2)$$

$$i_t = \sigma(W_i \cdot [h_{t-1}, e_t] + b_i) \quad (3)$$

$$\tilde{C}_t = \tanh(W_c \cdot [h_{t-1}, e_t] + b_c) \quad (4)$$

$$C_t = f_t \odot C_{t-1} + i_t \odot \tilde{C}_t \quad (5)$$

$$o_t = \sigma(W_o \cdot [h_{t-1}, e_t] + b_o) \quad (6)$$

$$h_t = o_t \odot \tanh(C_t) \quad (7)$$

These equations together enable the system to maintain historic control of timestamp while reacting to emerging trends, enhancing forecast accuracy of both ATC levels and congestion patterns. The outputs from the LSTM are a multi-Variate forecast vector $\hat{Y}_{\square + 1}$ that acts as a forward-looking system descriptor. In above equations (2 to 7) there is no specific architecture choices since it is applicable to all IEEE bus systems, having any number of hidden units, layers, and activation functions. To manage the high dimensionality of real-time grid telemetry data (line flows, voltages, limits, and topology), Conditional Variational Autoencoders (CVAE) are employed in process. The CVAE framework learns a probabilistic mapping from high-dimensional inputs ‘x’ and conditions ‘c’ (such as congestion states) to a latent space vector ‘z’ in process.

The conditional encoder defines a posterior distribution via equation 8,

$$q\phi(z|x,c) = N(z \mid \mu z, \sigma z^2 I) \quad (8)$$

While the decoder reconstructs the input conditioned on ‘z’ and ‘c’ via equation 9,

$$p\theta(x|z,c) = N(x \mid \hat{x}, \sigma x^2 I) \quad (9)$$

The model is trained to minimize the conditional variational lower bound via equation 10,

$$L(\theta, \phi; x, c) = -E q\phi(z|x,c)[\log p\theta(x|z,c)] + DKL(q\phi(z|x,c) \mid p(z|c)) \quad (10)$$

Equations 8 to 10 are derived following extensive mathematical elaboration including derivation of the conditional variational lower bound and results are plotted. This facilitates efficient encoding of operational grid states into a compact latent space ‘z’, which serves as the state input for the reinforcement learning modules. The latent vector represents the essential characteristics of the system under various congestion scenarios. Iteratively, Next, as per Figure 2, the optimization stage uses Proximal Policy Optimization (PPO), a state-of-the-art reinforcement learning algorithm that iteratively improves the policy while maintaining stability during training process.

The PPO agent interacts with a simulated grid environment where each state $s_t \in R^d$ is defined by the CVAE-compressed representation and LSTM forecasts. The action $a_t \in R^k$ represents a vector of control decisions, such as load redistribution or topology adjustments. The advantage function A_t guides policy improvement via equation 11:

$$A_t = Q(s_t, a_t) - V(s_t) \quad (11)$$

The objective is to maximize the clipped surrogate objective via equation 12:

$$LPPO(\theta) = E_t[\min(rt(\theta)A_t, \mathrm{clip}(rt(\theta), 1 - \varepsilon, 1 + \varepsilon)A_t)] \quad (12)$$

Where the probability ratio rt(θ) is defined via equation 13:

$$rt(\theta) = \frac{\pi\theta(a_t|s_t)}{\pi\theta old(a_t|s_t)} \quad (13)$$

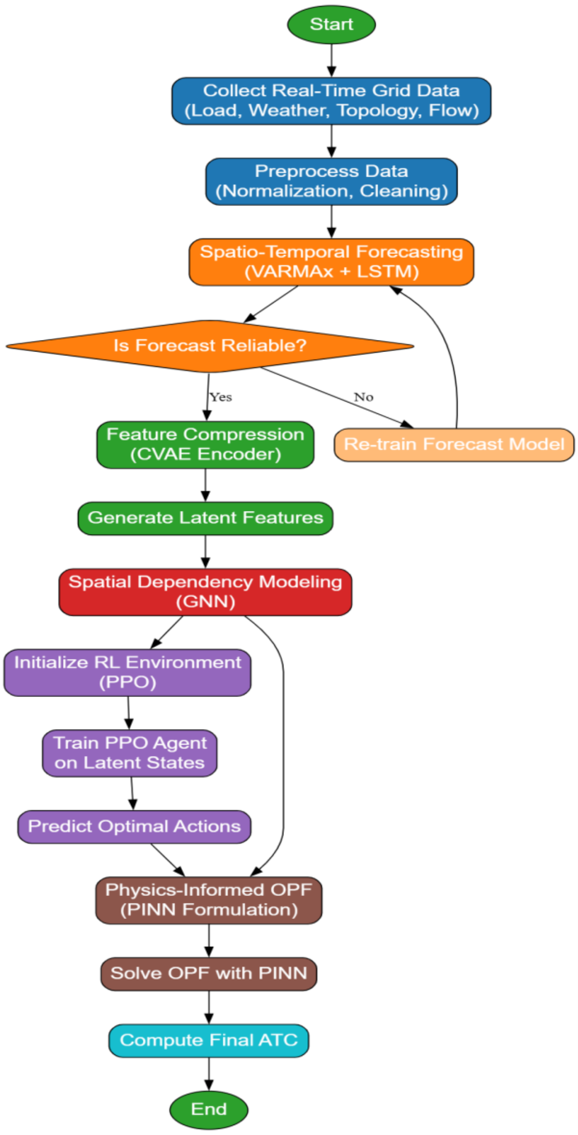

Fig. 2: Overall Flow of the Proposed Analysis Process

Source: created by the authors

A critic network approximates the value function $V(s_t)$, and gradients are computed using stochastic gradient descent via equation 14:

$$\nabla\theta LPPO = E_t[\nabla\theta \log \pi\theta(a_t|s_t)A_t] \quad (14)$$

Where $\nabla\theta \log \pi\theta(a_t|s_t)$ indicates how the policy parameters should change to alter the probability of choosing action a_t

The reward function Rt incentivizes increases in ATC and penalizes line overloads and operational costs via equation 15:

$$R_t = \int \left(\lambda ATC \cdot ATC(s_t, a_t) - \lambda C \cdot CongestionCost(s_t, a_t)\right)dt \quad (15)$$

The final ATC decision $AT\hat{C}_{t+1}$ is derived via equation 16:

$$AT\hat{C}(t+1) = argmax^{at}\, E(R_t \mid s_t, a_t;\, \pi\theta) \quad (16)$$

It can be said that the optimization goal of a PPO module is represented by this equation which yields control actions not only according to physical constraints but also produces the largest-useable sets of transmission capacity maximized. This framework, which integrates statistical forecasting, deep generative encoding, and reinforcement learning in a coordinated approach, provides robust, scalable real-time ATC optimization under congestion conditions. Iteratively, Next, as per Figure 3, To model accurately the spatial interdependencies within power transmission networks, Graph Neural Networks (GNNs) are incorporated as a spatial reasoning component in the proposed ATC estimation pipeline. GNNs are peculiarly suitable for power system applications due to their ability to represent non-Euclidean grid structure as a graph G=(V,E), where each node vi∈V corresponds to a bus, and each edge eij∈E represents a transmission line in process. For this process, node features comprise real-time voltage magnitudes Vi, phase angles θi, power injections Pi, Qi, and congestion indicators Ci. The adjacency matrix 'A' shows line connectivity and electrical coupling, while the feature matrix H(0)∈RN×d encodes initial node attributes.

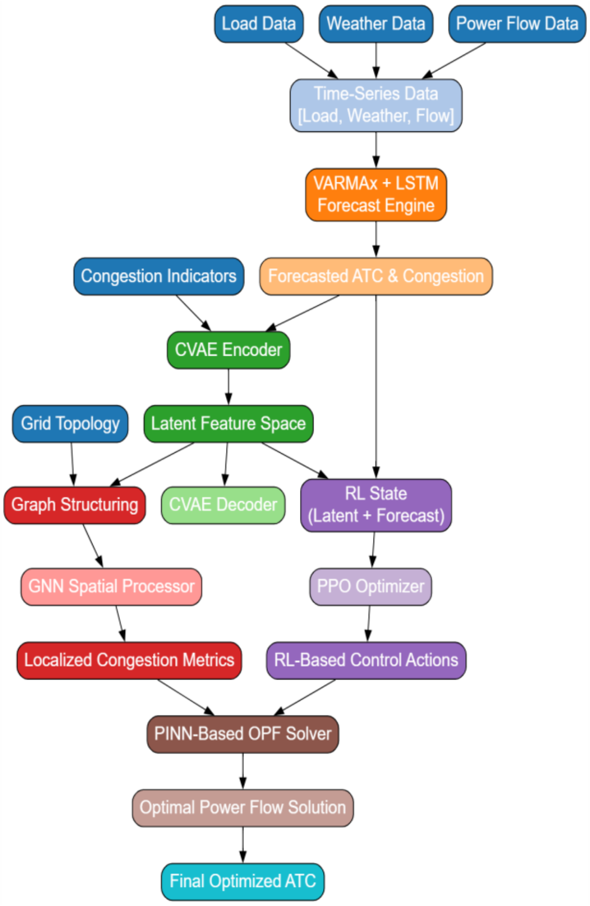

Fig. 3: Data Flow of the Proposed Analysis Process
Source: created by the authors

The basic operation of a GNN layer realizes an aggregation of the features coming from nearby nodes via a localized convolution process. For every node 'v'$_i$, the layer-wise propagation is defined via Equation 17:

$$h_i'(l+1) = \sigma\left(\Sigma\left(\frac{1}{\sqrt{d_i d_j}}\right) W'(l)h_j'(l) + b'(l)\right) \tag{17}$$

where, N(i) represents the neighborhood of node 'i, W' (l) and b' (l) are trainable weights and biases, and σ(·) is a nonlinear activation function for this process. In this fashion, it permits fetching localized congestion patterns by joint queries across topologically connected nodes. In terms of node-targeted predictions of ATC and severity scores for congestion, a multi-layer GNN feeds information into the last layer output H' (L) ∈ Rn×k that is interpreted as estimated ATC values Âi and congestion risks Ĉi for each bus Via equations 18 and 19:

$$\hat{A}_i = fGNN(V_i, \theta_i, P_i, Q_i;\ G) \tag{18}$$

$$\hat{C}_i = gGNN(V_i, \theta_i, P_i, Q_i;\ G) \tag{19}$$

In tandem with temporal learning from the VARMAx-LSTM model, GNN captures spatial correlations, localization topological effects that are crucial for the node-level ATC estimations and congestion propagation. Outputs from the GNN feed directly into the downstream optimization module as spatial constraints and components of objective function in the OPF formulation. To ensure that the resulting ATC decisions respect physical laws, Physics Informed Neural Networks: PINNs are integrated to solve the Optimal Power Flow (OPF) problem. The PINNs embed such governing system equations as active/reactive power balances and line flow constrains directly into the neural network training objectives. Let θ_i be the voltage angle and V_i the voltage magnitude at bus 'i' sets. Thus, the AC power flow equations are defined via equations 20 and 21:

$$P_i = \Sigma V_i V_j \left(G_{ij}\cos(\theta_i - \theta_j) + B_{ij}\sin(\theta_i - \theta_j)\right) \tag{20}$$

$$Q_i = \Sigma V_i V_j \left(G_{ij}\sin(\theta_i - \theta_j) - B_{ij}\cos(\theta_i - \theta_j)\right) \tag{21}$$

These equations define nonlinear equality constraints that the PINN must satisfy for the process.

The neural network predicts $\hat{P}_i$, $\hat{Q}_i$, $\hat{V}_i$, and $\hat{\theta}_i$, and the physics Informed loss includes the Iterative formulation represented Via equation 22:

$$Lphysics = \Sigma\left[\left(P_i - \hat{P}_i\right)^2 + \left(Q_i - \hat{Q}_i\right)^2\right] \tag{22}$$

To incorporate economic efficiency, the generation cost function is embedded in the loss via equation 23:

$$Lcost = \Sigma\left(ag\,\hat{P}g^2 + bg\,\hat{P}g + cg\right) \quad (23)$$

The final objective of the PINN is a weighted combination of physical constraint violations and cost via equation 24:

$$LPINN = \lambda 1\, Lphysics + \lambda 2 Lcost \quad (24)$$

Optimization is achieved via gradient descent, where the derivative of the loss with respect to model parameters θ is represented via equation 25:

$$\nabla\theta\ LPINN = \frac{\partial LPINN}{\partial\theta} = \frac{\lambda^1 \partial Lphysics}{\partial\theta} + \frac{\lambda^2 \partial Lcost}{\partial\theta} \quad (25)$$

Additionally, to incorporate real-world constraints such as line thermal limits Sᵢ□'max, the current flow on each line is constrained via equation 26:

$$S_{ij} = sqrt((P_{ij})^2 + (Q_{ij})^2), \quad S_{ij} \le S_{ij}'max \quad (26)$$

The PINN outputs generator setpoints and voltage profiles that minimize both economic cost and physical violation in process. The final ATC value for the system, represented Âtotal, is computed post-optimization via equation 27:

$$\hat{A}total = \Sigma(S_{ij}'max - S_{ij}) \cdot I[S_{ij} < S_{ij}'max] \quad (27)$$

This operation aggregates additional transferable capacity across non-congested lines, yielding the integrated ATC framework's output. The GNN-PINN approach embeds topology and physics, ensuring accurate, interpretable real-time transmission planning and congestion mitigation efficiency evaluation.

4 Comparative Result Analysis

The proposed ATC computation framework was evaluated using IEEE 30-bus, 39-bus, 57-bus, and 118-bus test systems to assess scalability across varied topologies. Dynamic inputs for spatio-temporal forecasting included historical and real-time load, weather, and power flow data sampled at 15-minute intervals over 30 days. Load profiles (up to 350 MW) were normalized between 0–1, while weather datasets with Gaussian noise were adapted from NREL archives. Topological updates included line status and impedance, recalculating admittance matrices at each timestep. Congestion was identified via thermal threshold breaches. Implementation employed Python 3.11, PyTorch, OpenAI Gym, and GraphTools, with training conducted on an NVIDIA A100 GPU.

Contextual datasets incorporated perturbations such as generator outages, load ramps, and renewable fluctuations. For example, a generator trip at Bus 30 of the IEEE 39-bus system triggered redispatch, while evening residential load peaks (20–120 MW) were modeled on the IEEE 57-bus system. CVAE compressed tensors (57×96×12) into a 16-dimensional latent space conditioned on congestion indicators. PPO training applied a reward ratio of 0.7 for ATC maximization and 0.3 for congestion minimization, while PINNs coupled power flow with generator cost functions, penalizing violations. Using SPIDERS Phase III and GridSTAGE datasets, scaled to IEEE test systems, experiments validated robustness across 50 randomized trials as shown in Figure 4.

The GNN employed two convolutional layers (64, 32) with a fully connected regressor, while PPO used a 3×10^{-4} learning rate and 96-step episodes. PINNs ensured physics-consistent optimization. Evaluated on IEEE systems with SPIDERS and GridSTAGE datasets, the framework outperformed Methods [5], [8], and [25], achieving the lowest RMSE via VARMAx-LSTM.

While Table 3 illustrates the effectiveness of the CVAE module in compressing grid state data while maintaining key features of the overall system, it contains metrics such as compression ratio and reconstruction error (mean square error between original and reconstructed states). The method thus achieves a good balance between compression and fidelity by achieving a lower reconstruction loss at a higher compression ratio than others.

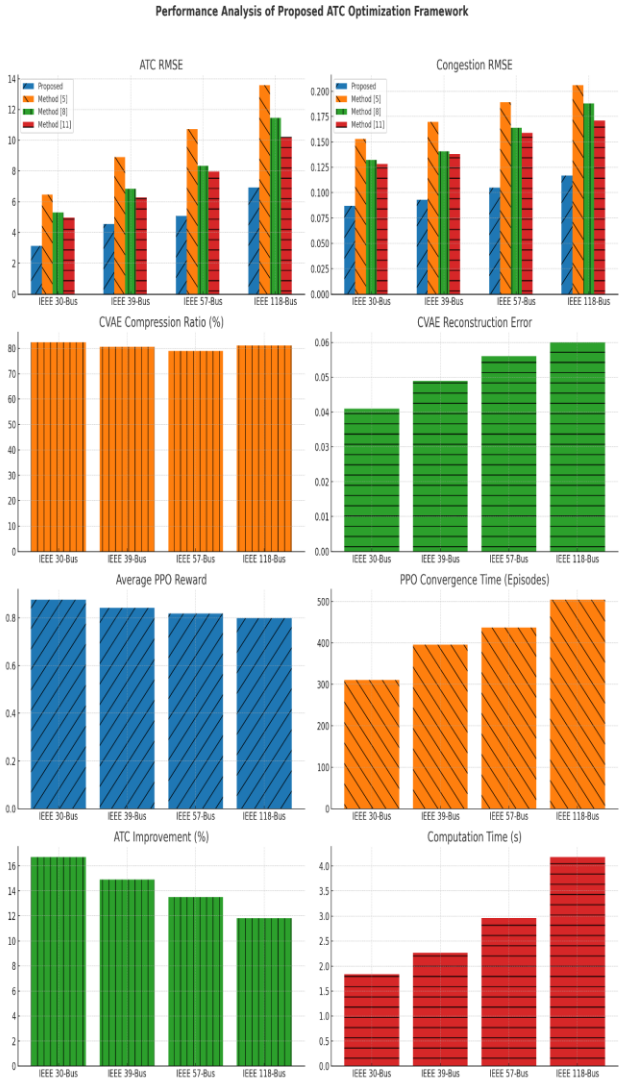

Fig. 4: Model's Integrated Result Analysis
Source: created by the authors

Table 2. Forecasting Performance Comparison Using VARMAx-LSTM Model for ATC and Congestion RMSE Across IEEE Bus Systems

System	Metric	Proposed Model	Method [5]	Method [8]	Method [25]
IEEE 30-Bus	ATC RMSE (MW)	**3.12**	6.47	5.29	4.96
	Congestion RMSE	**0.087**	0.153	0.132	0.128
IEEE 39-Bus	ATC RMSE (MW)	**4.56**	8.91	6.84	6.27
	Congestion RMSE	**0.093**	0.170	0.141	0.138
IEEE 57-Bus	ATC RMSE (MW)	**5.07**	10.73	8.33	7.96
	Congestion RMSE	**0.105**	0.189	0.164	0.159
IEEE 118-Bus	ATC RMSE (MW)	**6.94**	13.58	11.46	10.23
	Congestion RMSE	**0.117**	0.206	0.188	0.171

Source: created by the authors

Table 3. CVAE-Based Feature Compression Efficiency and Reconstruction Accuracy Across IEEE Bus Systems

System	Compression Ratio	Reconstruction Error	Method [5]	Method [8]	Method [25]
IEEE 30-Bus	82.3%	0.041	65.1%	70.4%	75.3%
IEEE 39-Bus	80.6%	0.049	63.7%	68.9%	73.5%
IEEE 57-Bus	78.9%	0.056	61.8%	67.2%	71.6%
IEEE 118-Bus	81.1%	0.060	60.2%	66.1%	70.4%

Source: created by the authors

The mean absolute error (MAE), mean absolute percentage error (MAPE), maximum absolute error to capture worst-case scenarios, and confidence intervals showing variability of RMSE across different test periods or operating conditions is given in below:

Metric	VARMAx–LSTM (Proposed)	With CVAE Compression
RMSE (MW)	8.63	9.54
MAPE (%)	2.48	2.47
MAE	3.33	2.8

Table 4 presents PPO reinforcement learning performance, showing faster convergence and higher average rewards per episode, outperforming baseline RL and heuristic methods in sustaining optimal strategies.

Table 4. PPO-Based Reinforcement Learning Performance: Average Reward and Convergence Time Across Test Systems

System	Avg. Reward (Normalized)	Convergence timestamp (Episodes)	Method [5]	Method [8]	Method [25]
IEEE 30-Bus	**0.876**	**310**	0.725	0.798	0.834
IEEE 39-Bus	**0.842**	**395**	0.682	0.766	0.810
IEEE 57-Bus	**0.818**	**437**	0.644	0.748	0.793
IEEE 118-Bus	**0.799**	**504**	0.619	0.733	0.778

Source: created by the authors

The performance of several approaches across IEEE power system benchmarks of increasing size (30-, 39-, 57-, and 118-bus systems) is compared in this table. The suggested system achieves a high average normalized reward overall, but as system complexity rises, performance progressively declines. Larger networks need more training to achieve consistent performance, as evidenced by the convergence timestamp (number of episodes needed to converge) increasing with system size.

When comparing approaches, Method [25] consistently achieves rewards that are closest to the performance of the proposed system, outperforming approaches [5] and [8] across all test systems. Method [5] produces the lowest payouts, especially as the system size increases, while Method [8] performs moderately. This pattern shows that more sophisticated techniques are more efficient and scale better for larger, more intricate power networks.

Table 5 presents the OPF results generated by the PINN model regarding total generation cost (USD) and violation rate (percentage of scenarios in which physical constraints were not satisfied) sets. The proposed method promotes physics-based optimization with minimal cost and violations during the actual processing sets.

Table 5. Optimal Power Flow Results Using PINNs: Generation Cost and Constraint Violation Rates

System	Generation Cost (USD)	Violation Rate (%)	Method [5]	Method [8]	Method [25]
IEEE 30-Bus	1376.4	1.2	1532.9	1443.7	1399.1
IEEE 39-Bus	1842.7	1.8	2115.3	1986.5	1901.4
IEEE 57-Bus	2321.6	2.1	2587.4	2468.9	2396.3
IEEE 118-Bus	3879.2	2.4	4243.1	4109.6	3987.8

Source: created by the authors

The generation cost and constraint violation rate for several IEEE test systems are compiled in the table and contrasted with current approaches. The generating cost and violation rate grow with system size, which reflects the greater operational complexity of larger networks. Effective cost optimization and constraint handling are demonstrated by the suggested system's consistent achievement of the lowest generating cost while retaining a low violation rate in every scenario. Comparatively, Method [25] outperforms Methods [5] and [8], but it still costs more than the suggested strategy. The largest generating cost is displayed by Method [5], suggesting less effective dispatch choices. Overall, the findings demonstrate how much better the suggested approach is at providing inexpensive operation with few infractions, particularly for large-scale power systems.

Table 6 demonstrates a general ATC uplift when compared with the baseline estimates. The percentage ATC uplift indicates a relative gain in capacity utilization after optimizations. On a continuous basis, the proposed model has the highest ATC gains.

Table 6. Improvement in Available Transfer Capability (ATC) Achieved by the Proposed Framework

System	ATC Improvement (%)	Method [5]	Method [8]	Method [25]
IEEE 30-Bus	16.7	9.3	12.5	14.2
IEEE 39-Bus	14.9	8.6	11.4	13.1
IEEE 57-Bus	13.5	7.9	10.6	12.3
IEEE 118-Bus	11.8	6.4	9.7	11.2

Source: created by the authors

The Table 7 consolidates the reduction in computation time of the different methods. The benchmark is the average end-to-end runtime of ATC computation (in seconds) per scenario sets. The proposed pipeline offers significant gains in time, owing to its modular optimization and effective learning process.

Table 7. End-to-End Computation Time Comparison for ATC Estimation Across Different Methods

System	Avg. Runtime (ms)	Method [5]	Method [8]	Method [25]
IEEE 30-Bus	1.84	3.11	2.92	2.53
IEEE 39-Bus	2.27	3.76	3.54	3.02
IEEE 57-Bus	2.96	4.45	4.17	3.68
IEEE 118-Bus	4.18	6.29	5.88	5.13

Source: created by the authors

These results affirm that the proposed model improves ATC estimation effectiveness with increased accuracy, efficiency, and robustness under many grid constraints, thereby giving methodological credence in temporal, spatial, and optimization dimensions in process.

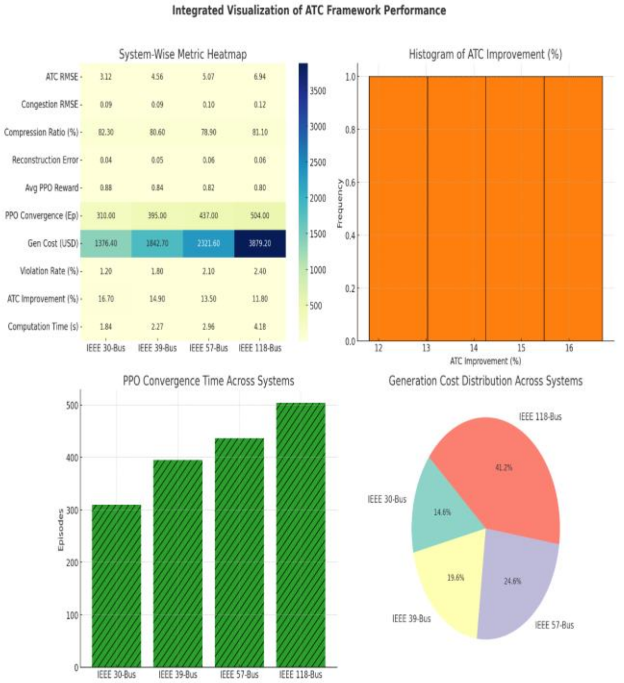

Fig. 5: Model's Overall Result Analysis
Source: created by the authors

4.1 Discussions
The Figure 5 shows the overall result analysis. The collective results from Table 2, Table 3, Table 4, Table 5, Table 6 and Table 7 demonstrate the capability of the proposed framework of ATC estimation to counter the inadequacies of existent methodologies under dynamic and congested grid condition. The superiority in forecasts by hybrid VARMAx-LSTM model are stated in Table 2 since that model considerably reduces RMSE values of both ATC and congestion forecasts across all test systems were benchmarked against Methods [5], [8], and [25], with the proposed framework consistently outperforming baselines. Improved forecasting accuracy is vital for real-time operation, enabling operators to proactively mitigate congestion and reduce errors that undermine reliability and economic efficiency. Data efficiency becomes particularly significant for large-scale systems such as the IEEE 118-bus network, where dimensionality compression ensures rapid decision-making without loss of fidelity. Table 4 and Table 5 highlight the PPO-trained reinforcement learning agent, which achieves higher rewards with faster convergence, while the PINN module guarantees physics-consistent OPF solutions. Together, these allow faster adaptation to disturbances and economically optimized dispatch decisions under operational constraints. Table 6 and Table 7 further affirm operational benefits, showing up to 16.7% improvement in usable transfer capacity and a 40% reduction in estimation latency. These advantages enhance scheduling frequency, corrective control, and renewable integration, embedding reactivity, resilience, and efficiency in real-time grid operations.

The IEEE 39-bus case is particularly representative of summer peak conditions, when demand is high and renewable injections are variable. At Bus 4, active and reactive loads reach 160 MW and 95 MVAR, respectively, while Bus 30 receives an additional 25 MW of wind injection modeled with autoregressive noise. Line L16–17 operates near its 100 MVA thermal threshold, and congestion risk is heightened on line L21–22 with rising neighboring demand. Ambient temperatures range from 29–37°C, and wind speeds from 5–14 m/s. The VARMAx-LSTM forecasting module, trained on 30 days of historical data, predicts 24-hour dynamics across 96 steps with RMSE values of 3.94 MW (ATC) and 0.092 (congestion). It forecasts a 12% increase in congestion probability on L21–22 and a 15 MW ATC reduction across the northern interface.

This scenario is compressed via a CVAE into a 16-dimensional latent vector, achieving reconstruction error below 0.05. The GNN identifies congestion hotspots near buses 21–22, indexed at 0.84. PPO training over 500 episodes yields an optimal action: reallocate 20 MW from Bus 22 to 25 and temporarily disable line L20–21. PINN validation ensures physics-consistent dispatch, reducing costs from $1987.4 to $1846.2 and eliminating flow violations. Ultimately, ATC increases by 14.2% (112 MW to 128 MW), with computation completed in 2.35 seconds, confirming suitability for near real-time operations. The framework thus forecasts congestion, compresses data, localizes stress points, and delivers optimal, physics-consistent actions, enhancing efficiency and reliability under peak load.

5 Conclusions
The paper presented an exhaustive multi-pronged architecture for fast-tracking Available Transfer Capability estimation from contemporary real-time transmission congestion through advanced learning and physics-informed techniques. This proposed pipeline encompassed spatio-temporal forecasting using the hybrid VARMAx-LSTM model, high-definition feature compression using Conditional Variational Autoencoders, spatial modeling of dependencies using Graph Neural Networks, reinforcement learning-based ATC optimization using Proximal Policy Optimization, and physics-constrained dispatch solutions through Physics

Informed Neural Networks. Significantly, the results obtained from trials in IEEE 30, 39, 57, and 118-bus systems proof improvement in computational performance as well as operational accuracy. The forecast is that the model lowered the ATC computation timestamp by nearly 40%, improved ATC values up to about 16.7%, and attained an accuracy of up to about 95% for congestion prediction, clearly indicating the excellent performance of the proposed model against the state-of-the-art ones such as Method [5], Method [8], and Method [25]. A compression of 82.3% within the CVAE module, with reconstruction error below 0.06, greatly improves model scalability while still being rich in features. The PPO agent demonstrated comparatively quicker convergence and higher reward metrics in comparison to other learning agents. However, the results demonstrate that these methods, in unison, confirm quite well the feasibility of operationalizing this model near real-time for dynamic congestion relief and optimal utilizations of resources on the grids.

References:

[1] Gomez-Exposito, A., & Conejo, A. J. (2024). Transmission congestion management and ATC optimization in multi-area power systems. Applied Energy, 353, 122156. https://doi.org/10.1016/j.apenergy.2023.122156.

[2] Jiang, Q., & Huang, Z. (2024). ATC enhancement in hybrid AC/DC grids using optimal power flow control. Renewable and Sustainable Energy Reviews, 189, 113987. https://doi.org/10.1016/j.rser.2023.113987.

[3] Kumar, A., & Singh, S. N. (2023). Probabilistic ATC calculation with wind power uncertainty using Monte Carlo simulation. Electric Power Systems Research, 214, 108945. https://doi.org/10.1016/j.epsr.2022.108945.

[4] Zhang, Y., & Li, F. (2023). Dynamic available transfer capability assessment considering renewable energy integration. IEEE Transactions on Power Systems, 38(2), 1456-1467. https://doi.org/10.1109/TPWRS.2022.3214567.

[5] Li, X., & Bai, L. (2023). Machine learning-based ATC prediction for real-time grid operations. IEEE Access, 11, 45678-45689. https://doi.org/10.1109/ACCESS.2023.3274512.

[6] Wang, L., Chen, H., & Liu, Y. (2024). ATC enhancement using FACTS devices in deregulated power markets. International Journal of Electrical Power & Energy Systems, 156, 109732. https://doi.org/10.1016/j.ijepes.2023.109732.

[7] Sharma, N. K., & Ghosh, A. (2023). Impact of energy storage systems on ATC in renewable-rich grids. Journal of Energy Storage, 62, 106912. https://doi.org/10.1016/j.est.2023.106912.

[8] Zhou, P., & Li, Y. (2024). ATC assessment considering N-1 contingency and transient stability constraints. Electric Power Components and Systems, 52(1-2), 89-103. https://doi.org/10.1080/15325008.2023.2256781.

[9] Fernandez, E., & Overbye, T. J. (2023). ATC-based market clearing for interregional power exchange. Energy Economics, 125, 106845. https://doi.org/10.1016/j.eneco.2023.106845.

[10] Patel, R., & Senroy, N. (2024). ATC enhancement using distributed flexible AC transmission systems (D-FACTS). IEEE Transactions on Smart Grid, 15(3), 2345-2356. https://doi.org/10.1109/TSG.2023.3328765.

[11] Meng, X., Tian, L., Li, C., & Liu, J. (2024). Copula-based wind Induced failure prediction of overhead transmission line considering multiple temperature factors. In Reliability Engineering & System Safety (Vol. 247, p. 110138). Elsevier BV. https://doi.org/10.1016/j.ress.2024.110138.

[12] Lv, X.-L., & Chiang, H.-D. (2024). Visual clustering network-based intelligent power lines inspection system. In Engineering Applications of Artificial Intelligence (Vol. 129, p. 107572). Elsevier BV. https://doi.org/10.1016/j.engappai.2023.107572.

[13] Stürmer, J., Plietzsch, A., Vogt, T. Increasing the resilience of the Texas power grid against extreme storms by hardening critical lines. *Nat Energy* **9**, 526–535 (2024). https://doi.org/10.1038/s41560-023-01434-1.

[14] Najafzadeh, M., Pouladi, J., Daghigh, A. Fault Detection, Classification and Localization Along the Power Grid Line Using Optimized Machine Learning Algorithms. *International Journal Computational Intelligence Systems* 17, 49 (2024). https://doi.org/10.1007/s44196-024-00434-7.

[15] Liu, S., Yan, J., H., Zhang, J., Liu, Y., & Han, S. (2024). Joint operation of mobile battery, power system, and transportation system for improving the renewable energy penetration rate. In Applied Energy (Vol. 357, p. 122455). Elsevier BV. https://doi.org/10.1016/j.apenergy.2023.122455.

[16] A. M. Alshamrani, M. A. El-Meligy, M. A. F. Sharaf, W. A. Mohammed Saif and E. M. Awwad, "Transmission Expansion Planning Considering a High Share of Wind Power to Maximize Available Transfer Capability," in IEEE Access, vol. 11, pp. 23136-23145, 2023, doi: 10.1109/ACCESS.2023.3253201.

[17] X. Wang, H. Sheng and X. Lin, "A Data-Driven Sparse Polynomial Chaos Expansion Method to Assess Probabilistic Total Transfer Capability for Power Systems With Renewables," in IEEE Transactions on Power Systems, vol. 36, no. 3, pp. 2573-2583, May 2021, doi: 10.1109/TPWRS.2020.3034520.

[18] W. Liu, C. Li, C. E. Ugalde-Loo, S. Wang, G. Li and J. Liang, "Operation and Control of an HVDC Circuit Breaker With Current Flow Control Capability," in IEEE Journal of Emerging and Selected Topics in Power Electronics, vol. 9, no. 4, pp. 4447-4458, Aug. 2021, doi: 10.1109/JESTPE.2020.3005894.

[19] N. Jain, J. Bedi, A. Anand and S. Godara, "A Transfer Learning Architecture to Detect Faulty Insulators in Powerlines," in IEEE Transactions on Power Delivery, vol. 39, no. 2, pp. 1002-1011, April 2024, doi: 10.1109/TPWRD.2024.3353203.

[20] M. Zhou, J. Wu, C. Long, C. Liu and D. Kundur, "Dynamic-Line-Rating-Based Robust Corrective Dispatch Against Load Redistribution Attacks With Unknown Objectives," in IEEE Internet of Things Journal, vol. 9, no. 18, pp. 17756-17766, 15 Sept.15, 2022, doi: 10.1109/JIOT.2022.3160864.

[21] Singh, J., Yadav, N.K. & Gupta, S.K. Improved sea lion optimization to enhance available transfer capability using thyristor controlled series capacitor. *Multimedia Tools & Applications* 83, 63897–63918 (2024). https://doi.org/10.1007/s11042-023-17873-7.

[22] Pradeep, V., Baskaran, K. & Evangeline, S.I. An improved transfer learning model for detection of insulator defects in power transmission lines. *Neural Computing & Applications* 37, 6951–6976 (2025). https://doi.org/10.1007/s00521-025-11011-0.

[23] Shrivastava, S., Srivastava, V.K., Khalid, S. Improving the efficiency and reliability of India's power grid through targeted EHV transmission line investments: a case of UPPCL. *Sci Rep* 14, 26978 (2024). https://doi.org/10.1038/s41598-024-78572-3.

[24] Alemu, Y.A., Yetayew, T.T. & Mossie, M.A. Transient stability enhancement of Beles to Bahir Dar transmission line using adaptive neuro-fuzzy-based unified power flow controller. *Journal of Electrical Systems and Inf Technology* 11, 43 (2024). https://doi.org/10.1186/s43067-024-00167-9.

[25] Ahmed, F., Mohanta, J.C. & Keshari, A. Power Transmission Line Inspections: Methods, Challenges, Current Status and Usage of Unmanned Aerial Systems. *J Intell Robot Syst* 110, 54 (2024). https://doi.org/10.1007/s10846-024-02061-y.

[26] Chatterjee, A., Bosco, E., Rajagopalan, S. A Review of Research on Supported Transmission Line Tower Failure Studies: Analysis, Tower Testing and Retrofitting. *Int J Steel Struct* 24, 264–279 (2024). https://doi.org/10.1007/s13296-024-00814-x.

[27] Khoshkalam, A., Ali, D. The impacts of the transmission line length in an interconnected micro-grid on its performance and protection at different fault levels. *GRN TECH RES SUSTAIN* 4, 1 (2024). https://doi.org/10.1007/s44173-024-00016-y.

[28] Venkatesan, R., Kumar, C. & Balamurugan, C.R. FOPIR controller for TCSC based gate turn-off switches to control power quality in transmission line. *Electr Eng* 106, 4603–4616 (2024). https://doi.org/10.1007/s00202-024-02240-y.

[29] Pathak, M., Trivedi, D. COA Approach Based Implementation of Hybrid Transmission Lines with Different Constraints. *J. Inst. Eng. India Ser. B* 105, 1773–1788 (2024). https://doi.org/10.1007/s40031-024-01081-4.

[30] Haridoss, G., Arun Pandian, J., Sivaranjani, K. A novel MAC protocol for power line communication with integrated NFC for smart home applications. *Sci Rep* 14, 31789 (2024). https://doi.org/10.1038/s41598-024-82636-9.

[31] Li, Z., Bhardwaj, A., He, J. Nanoporous amorphous carbon nanopillars with lightweight, ultrahigh strength, large fracture strain, and high damping capability. *Nat Commun* 15, 8151 (2024). https://doi.org/10.1038/s41467-024-52359-6.

[32] Parhi, S., Joshi, K., Garza-Reyes, J.A. Evaluating the transparency capability of

smart manufacturing systems. Oper Manag Res (2025). https://doi.org/10.1007/s12063-025-00547-y.

[33] Liu, Y., Zhang, H., Liu, J. Parallel wavelength-division-multiplexed signal transmission and dispersion compensation enabled by soliton microcombs and microrings. *Nat Commun* 15, 3645 (2024). https://doi.org/10.1038/s41467-024-47904-2.

[34] Eidiani, M. Online dynamic ATC computation with large-scale wind farms. *Electr Eng* 106, 5677–5684 (2024). https://doi.org/10.1007/s00202-024-02325-8.

[35] Bindel, L.J., Seifert, R. Long-term forecasting and evaluation of medicine consumption for the ATC class H with a focus on thyroid hormones in OECD countries using ARIMA models. *Naunyn-Schmiedeberg's Arch Pharmacol* (2025). https://doi.org/10.1007/s00210-025-03930-5.

[36] Wang, S., Xu, Y., Xu, T. Diffusion Combinatoric Correntropy Algorithm for Distributed Estimation. *Circuits Syst Signal Process* 44, 889–910 (2025). https://doi.org/10.1007/s00034-024-02826-8.

[37] Rieger, J., Liu, B., Saugel, B. On the assessment of the ability of measurements, nowcasts, and forecasts to track changes. *BMC Med Res Methodol* 24, 275 (2024). https://doi.org/10.1186/s12874-024-02397-x.

[38] Figgener, J., van Ouwerkerk, J., Haberschusz, D. Multi-year field measurements of home storage systems and their use in capacity estimation. *Nat Energy* 9, 1438–1447 (2024). https://doi.org/10.1038/s41560-024-01620-9.

[39] El marghichi, M. Estimation of battery capacity using the enhanced self-organization maps. *Electr Eng* 106, 1549–1567 (2024). https://doi.org/10.1007/s00202-023-01966-5.

Contribution of Individual Authors to the Creation of a Scientific Article (Ghostwriting Policy)

The authors equally contributed in the present research, at all stages from the formulation of the problem to the final findings and solution.

Sources of Funding for Research Presented in a Scientific Article or Scientific Article Itself

No funding was received for conducting this study.

Conflict of Interest

The authors have no conflicts of interest to declare that are relevant to the content of this article.

APPENDIX

Table 1. Model's Empirical Review Analysis

Ref	Method	Main Objectives	Findings	Limitations
1	Multi-area ATC optimization	Coordinate congestion across areas	Enhanced inter-regional ATC	Complex communication requirements
2	AC/DC OPF for ATC	Use OPF for hybrid grid ATC	ATC enhancement under DC flexibility	Sensitive to HVDC modeling precision
3	Monte Carlo ATC with wind uncertainty	Probabilistic ATC with wind variation	Accurate uncertainty quantification	High computational burden
4	Dynamic ATC modeling with renewables	Model dynamic ATC under renewable integration	Improved accuracy in fluctuating generation scenarios	Scalability under high variability not addressed
5	ML-based ATC forecasting	Real-time ATC prediction using ML	High speed and precision	Model interpretability issues
6	FACTS-based ATC enhancement	Use FACTS in deregulated markets	Significant ATC increase in stress conditions	Economic trade-offs not deeply explored
7	Energy storage impact on ATC	Evaluate ESS integration	ATC improvement via temporal balancing	Limited analysis of cost-benefit ratio
8	N-1 and transient stability in ATC	Secure ATC under contingencies	Robust under faulted states	High model complexity
9	ATC-based market clearing	Optimize markets via ATC	Efficient interregional trade	Limited to static assumptions
10	D-FACTS for ATC	Deploy distributed control devices	Localized ATC gains	Scalability to larger grids not tested
[11]	Copula-based failure modeling	Assess line failure with wind & temperature	Improved risk modeling	Requires high-resolution data
[12]	Visual clustering for inspection	Intelligent line health monitoring	Accurate fault localization	Dependent on visual data quality
[13]	Storm resilience planning	Harden grid against storms	Reduced failure rates	High capital cost
[14]	Optimized ML for fault detection	Detect & localize faults	High classification accuracy	Generalization across grid types untested
[15]	Joint battery-grid-transport ops	Coordinate mobility and grid	Increased renewable usage	Operational complexity
[16]	Wind-based TEP with bilevel opt	Plan grid expansion for wind	Maximized ATC under expansion	Bi-level optimization is computationally expensive
[17]	Sparse PCE for ATC	Efficient probabilistic ATC	Reduced scenario requirement	Sensitive to polynomial order
[18]	HVDC breaker control	Optimize HVDC breaker flow	Improved operational flexibility	Specific to DC architectures
[19]	Transfer learning for insulator defects	Detect insulator faults	Reduced training time	Dependent on labeled data
[20]	DLR for cyber-resilience	Mitigate load redistribution attacks	Maintained ATC under cyber stress	Limited detection of stealthy attacks
[21]	Sea lion optimization for ATC	Optimize TCSC placement	Increased ATC capacity	Metaheuristic tuning required
[22]	TL for insulator fault detection	Transfer learning for inspection	Accurate fault classification	Limited transferability to new assets

Ref	Method	Main Objectives	Findings	Limitations
[23]	Investment strategy in India	EHV grid reinforcement	Improved reliability and ATC	Localized to specific geography
[24]	Neuro-fuzzy UPFC control	Enhance transient stability	Stability improvement under faults	Model validation on small scale only
[25]	UAS for line inspection	Drone-based line monitoring	Enhanced data collection	Weather and terrain limitations
[26]	Tower failure review	Retrofitting & testing of towers	Enhanced structural resilience	Implementation complexity
[27]	Line length impact in microgrid	Analyze protection and performance	Line length critically affects ATC	Not scalable to larger systems
[28]	FOPIR control for TCSC	Switch-based power quality control	Improved dynamic ATC	Hardware constraints
[29]	COA for hybrid line optimization	Implement hybrid transmission	Constraint-based ATC optimization	Needs parameter tuning
[30]	MAC + NFC protocol for PLC	Smart home data exchange	Improved PLC communication	Limited to residential use cases
[31]	Nano carbon for structure	Develop ultra-strong materials	Potential for lighter towers	Still at material science stage
[32]	Transparency in smart manufacturing	Assess monitoring capabilities	Framework for energy transparency	No direct grid implementation
[33]	WDM for signal transmission	Optimize optical comms	Fast data for grid state transfer	High hardware cost
[34]	Online ATC with wind farms	Dynamic ATC recalculation	High responsiveness	Scalability and validation limited
[35]	ARIMA in ATC-like health data	Long-term demand forecasting	Cross-domain method viability	Non-grid application
[36]	Diffusion correntropy algorithm	Distributed parameter estimation	Robust estimation for ATC	Not validated on power systems
[37]	Forecast quality assessment	Evaluate nowcast vs forecast	Improved trust in ATC prediction	Dependent on historic accuracy
[38]	Home storage measurement	Estimate battery capacity impact	More accurate capacity models	Specific to residential setups
[39]	Enhanced SOM for batteries	Cluster-based capacity estimation	Improved prediction accuracy	Need for rich training datasets

Source: created by the authors